









# Groundwater springs formed during glacial retreat are a large source of methane in the high Arctic

Received: 27 September 2022

Accepted: 22 May 2023

Published online: 6 July 2023

 Check for updates

Gabrielle E. Kleber <sup>1,2</sup>✉, Andrew J. Hodson <sup>2,3</sup>, Leonard Magerl <sup>4</sup>, Erik Schytt Mannerfelt <sup>2,5</sup>, Harold J. Bradbury <sup>1,6</sup>, Yizhu Zhu <sup>7</sup>, Mark Trimmer <sup>7</sup> & Alexandra V. Turchyn <sup>1</sup>

Permafrost and glaciers in the high Arctic form an impermeable ‘cryospheric cap’ that traps a large reservoir of subsurface methane, preventing it from reaching the atmosphere. Cryospheric vulnerability to climate warming is making releases of this methane possible. On Svalbard, where air temperatures are rising more than two times faster than the average for the Arctic, glaciers are retreating and leaving behind exposed forefields that enable rapid methane escape. Here we document how methane-rich groundwater springs have formed in recently revealed forefields of 78 land-terminating glaciers across central Svalbard, bringing deep-seated methane gas to the surface. Waters collected from these springs during February–May of 2021 and 2022 are supersaturated with methane up to 600,000 times greater than atmospheric equilibration. Spatial sampling reveals a geological dependency on the extent of methane supersaturation, with isotopic evidence of a thermogenic source. We estimate annual methane emissions from proglacial groundwaters to be up to 2.31 kt across the Svalbard archipelago. Further investigations into marine-terminating glaciers indicate future methane emission sources as these glaciers transition into fully land-based systems. Our findings reveal that climate-driven glacial retreat facilitates widespread release of methane, a positive feedback loop that is probably prevalent across other regions of the rapidly warming Arctic.

Globally relevant amounts of methane in subsurface natural gas deposits and coal beds of the Arctic<sup>1</sup> are assumed to be sealed beneath a perennially frozen ‘cryospheric cap’ of permafrost and glaciers<sup>2–5</sup>. At sufficiently high pressures and low temperatures, the methane beneath permafrost and glaciers can be trapped as a solid gas hydrate<sup>6</sup>.

These pressure and temperature conditions may shift with climate warming and glacial retreat, potentially causing the disintegration of gas hydrates and release of deep, subsurface methane to the Arctic atmosphere<sup>4,7–11</sup>. In cases where pressures are too low for gas hydrate stability, increased summer mass losses of glaciers are able to recharge

<sup>1</sup>Department of Earth Sciences, University of Cambridge, Cambridge, UK. <sup>2</sup>Arctic Geology, University Centre in Svalbard (UNIS), Longyearbyen, Norway.

<sup>3</sup>Department of Environmental Sciences, Western Norway University of Applied Sciences, Sogndal, Norway. <sup>4</sup>Department of Geology, UiT the Arctic University of Norway, Tromsø, Norway. <sup>5</sup>Department of Geosciences, University of Oslo, Oslo, Norway. <sup>6</sup>Department of Earth, Ocean and Atmospheric Sciences, University of British Columbia, Vancouver, British Columbia, Canada. <sup>7</sup>School of Biological and Behavioural Sciences, Queen Mary University of London, London, UK. ✉e-mail: [gabrielle.kleber@gmail.com](mailto:gabrielle.kleber@gmail.com)

groundwater aquifers beneath the permafrost and encourage the migration of gas to the surface<sup>12</sup>.

Permafrost degradation due to increasing Arctic air temperatures is slow relative to glacial retreat. In the case of land-terminating glaciers, glacial retreat can expose forefields (land that was previously covered by the glacier) with areas where permafrost is out of equilibrium with the climate and therefore either absent or discontinuous. These forefields provide an outlet for subpermafrost groundwaters that were previously sealed beneath the overburden glacier and permafrost and facilitate the formation of terrestrial methane seepage (Fig. 1). Mean annual air temperatures on Svalbard, a Norwegian archipelago in the high Arctic, are rising at a rate five to seven times faster than the global average and twice as fast as elsewhere in the Arctic<sup>13</sup>. Rising temperatures have led to a 30% volume loss of glaciers on Svalbard since 1936, which has been accompanied by a decrease in glacial coverage by about 10.4% (ref. 14). Increased summer ablation and rapidly expanding glacial forefields due to glacial retreat are causing new methane seepage pathways to form in association with proglacial groundwater springs. This study presents evidence that these seepage pathways induce widespread groundwater-driven methane escape from glacial forefields in the Eurasian High Arctic, a region known for its vast subpermafrost gas reserves<sup>1</sup>.

The onset of substantial glacial retreat on Svalbard near the start of the twentieth century<sup>15</sup> enabled gaps to form in the cryospheric cap between the retreating glacier margin and the encroaching permafrost boundary. These discontinuities provide outlets for pressurized groundwater systems formerly sealed by the pressure of glacial ice (Fig. 1). Aquifers within the sub- and proglacial sediments are recharged by snow and glacial melt during the summer, and artesian pressure releases water through a perennial groundwater spring. The groundwater flow path is maintained through advective heat transfer from the constant flow of water, even throughout winter, which inhibits the development of permafrost<sup>16,17</sup>. During the winter, freezing of successive groundwater outflows forms large, stratified icing fields in glacial forefields that can be several metres thick (Fig. 2). Formation of the icing releases latent heat through freezing of water, which further inhibits the advance of permafrost. This creates and maintains a talik (an unfrozen volume of water-saturated sediments) at the surface that can be sustained for many years. Proglacial icings are common on Svalbard<sup>18,19</sup> and are found in other glaciated regions of the Arctic and sub-Arctic<sup>17,20,21</sup>.

Methane may be introduced to these groundwater systems through a variety of mechanisms, thus exploiting their flow paths to reach the atmosphere. First, methane can be present as subsurface gas hydrates, whose dissociation occurs during glacial retreat. Thermobaric modelling has suggested that natural gas hydrates occur naturally onshore in central Svalbard<sup>22</sup>. Evidence of this mode of methane supply is observed in pockmarks in the vicinity of retreating ice streams<sup>9</sup> and has been linked to long-term methane evasion dynamics of permafrost sediments within valley systems in Svalbard<sup>23</sup>. Second, microbial methane production—methanogenesis—may take place in deeper groundwater flow paths that are recharged by high-elevation glacial or non-glacial meltwaters. Finally, the upward migration of methane from deep-seated biogenic or thermogenic sources may lead to gas accumulation beneath the glacier or permafrost, saturating the subglacial groundwater systems.

Although the Arctic is considered a substantial contributor of methane to the atmosphere<sup>24</sup>, current estimates do not yet include methane escaping from gas deep within or beneath permafrost. While the potential for methane release from these deeper sources is known to exist<sup>4,7</sup>, the magnitude and pathways of this release are uncertain. We undertook a field survey of unprecedented spatial coverage to identify methane emission hotspots in terrestrial glacial forefields, a previously unknown emission source. By measuring methane concentrations in proglacial groundwater springs in the forefields of 78 land-terminating

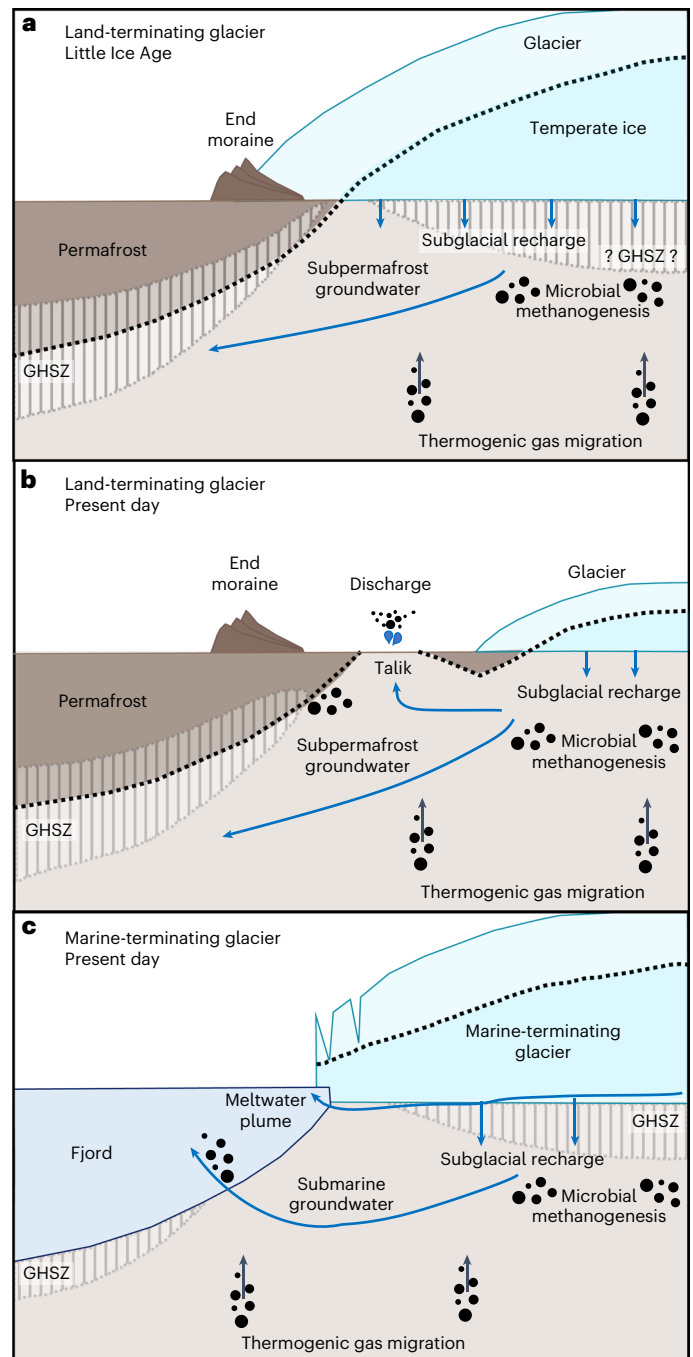


**Fig. 1 | Conceptual model of methane-rich proglacial groundwater springs associated with glacier–permafrost coupling. a**, A continuous cryospheric cap is formed by permafrost extending below land-terminating glacial termini during the later stages of the Little Ice Age on Svalbard (circa 1900). Hydrological connection from the subpermafrost groundwater system to the surface is limited. **b**, Land-terminating glaciers have retreated due to climate warming, exposing unfrozen ground. Methane-enriched groundwater discharges through proglacial springs. Permafrost develops as glaciers retreat further. However, advective heat associated with groundwater flow and latent heat released during winter icing formation prevent taliks from freezing, allowing continuous groundwater discharge through proglacial springs. Gas hydrate stability zones (GHSZs) are estimated on the basis of modelling by Betlem et al.<sup>22</sup>. **c**, Methane-rich subglacial groundwater beneath contemporary marine-terminating glaciers.

glaciers across central Svalbard, we estimate total methane emissions from these springs across the Svalbard archipelago. Furthermore, we complement our onshore survey with an offshore study of three

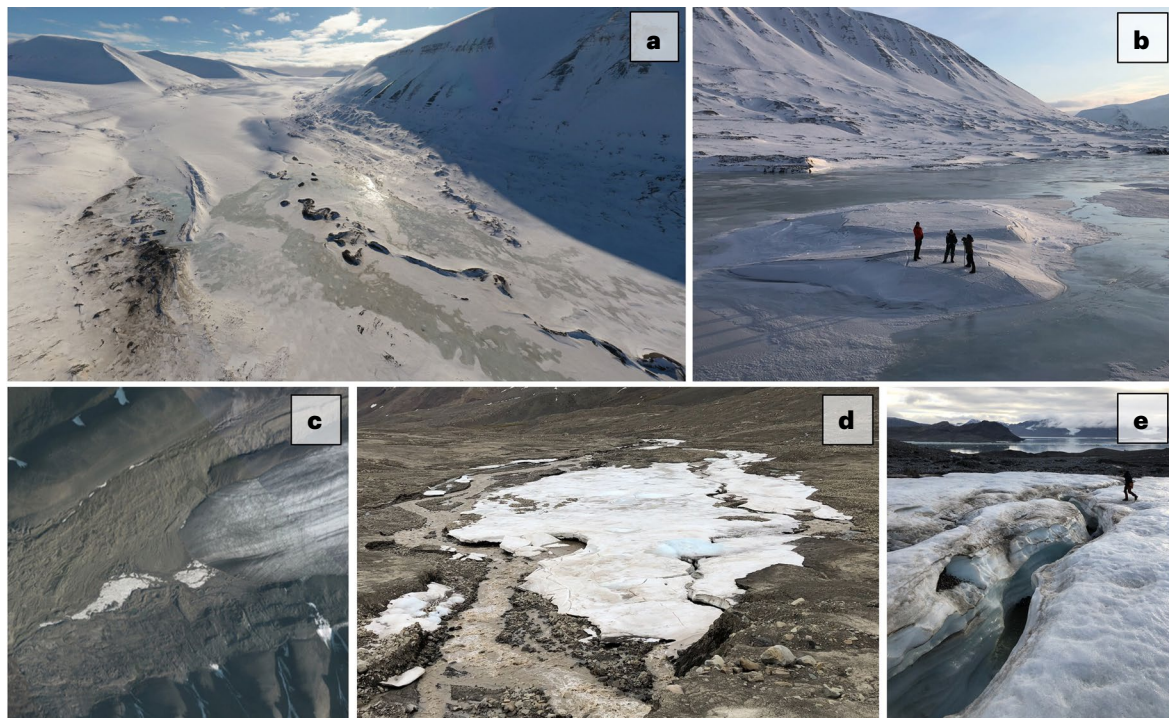


**Fig. 2 | Images of proglacial icings of land-terminating glaciers.** **a**, Drone image of a winter icing formed at the glacier margin and extending within the proglacial river floodplain. **b**, Ice blister formed within an icing due to pressurized groundwater flow during winter. **c**, Aerial image of glacier (right)

and icing remnants (left) in mid-summer. **d**, Icing field in early summer. **e**, Icing surface in summer with person for scale; ice layers formed by subsequent winter groundwater outflows are visible. Credit: photograph in **c**, Norwegian Polar Institute.

glaciers that terminate in the sea (marine-terminating glaciers) to consider emergent methane emissions from marine-terminating glaciers as they retreat far enough to transition into land-terminating glaciers.

### Methane supersaturation in proglacial groundwaters

Land-terminating valley glaciers in the high Arctic offer opportunities to sample pressurized outflows immediately upon their emergence in the glacial forefield, thus limiting the degassing of methane and other gases before sampling. Our analysis of 123 discrete groundwater springs, from 78 land-terminating glaciers across central Svalbard (Fig. 3a), reveals ubiquitous supersaturated methane-rich groundwater springs with concentrations more than 600,000 times greater than those in equilibrium with the atmosphere. Measured concentrations range from 0 to  $2.57 \times 10^6$  nM (mean:  $1.46 \times 10^5$  nM; median:  $1.25 \times 10^3$  nM), relative to an equilibrational concentration of  $-4.0$  nM (Fig. 4a). Excess methane above  $4.0$  nM begins to degas from the water upon reaching the surface and equilibrating with the atmosphere. All but one seep has methane concentrations greater than equilibrium, indicating that proglacial springs are a year-round source of methane to the Arctic atmosphere.

### Spatial sampling reveals geology-dependent methane seepage

The Svalbard archipelago is part of the uplifted northwestern margin of the Barents Shelf. The geology of central Svalbard (depicted in Fig. 3) contains a proven hydrocarbon system that extends both onshore and offshore<sup>25–31</sup>. Central Svalbard is dominated by the Central Tertiary Basin, a succession of sandstone and organic-rich shale accumulated during the Palaeocene and Eocene. The basin is linked to well-known natural seepages of methane associated with lowland pingos<sup>23</sup>. In the east, Jurassic and Triassic shale formations outcrop, which are onshore equivalents to prolific source rocks in the Barents Sea<sup>32,33</sup> and may be

connected to active pockmarks and subsea methane seeps<sup>26,28,34</sup>. The western edge of central Svalbard has contrasting geology, with uplifted Precambrian metamorphic basement rocks that have been folded against younger sedimentary layers.

While we found supersaturation of methane to be ubiquitous among our sampled proglacial groundwater springs, there is evidence that the outcropping geology controls the extent of this supersaturation. Statistical analysis indicates that bedrock geology significantly affects log-transformed methane concentrations (analysis of variance,  $F_{4,118} = 9.65, P < 0.001$ ), explaining approximately a quarter of the total variation in methane supersaturation across the sites ( $R^2 = 0.247$ ). Methane ‘hotspots’ are associated mostly with the shale-dominated Jurassic and Triassic units outcropping in the east (Tukey’s honestly significant difference pairwise comparison of means,  $P < 0.05$  for four out of six pairs; Supplementary Table 1), indicated in Fig. 3b and more substantially supported by sorting the data by outcropping geology in Fig. 4b.

The occurrence of high methane concentrations near shale outcrops suggests a geologic or thermogenic source of gas, which is able to migrate upwards and accumulate beneath the glacier due to fractures that increase the connectivity between pore spaces<sup>35</sup>. The gas exploits subglacial groundwater flow paths and is brought to the surface with proglacial groundwater springs, where it is emitted to the atmosphere. This theory is supported by the stable carbon isotopic compositions of methane in the samples ( $\delta^{13}\text{C}-\text{CH}_4$ ), which lie largely in the thermogenic range (Fig. 4c), ranging from  $-60.0$  to  $-32.0$ ‰ (mean  $\delta^{13}\text{C}-\text{CH}_4 = -46.5$ ‰,  $n = 36$ ). (Microbial methane typically varies in  $\delta^{13}\text{C}$  from  $-110$  to  $-50$ ‰, while thermogenic methane is less depleted in  $^{13}\text{C}$  and has a  $\delta^{13}\text{C}$  range from  $-50$  to  $-20$ ‰ (ref. 36.))

Thermogenic methane may be supplemented with microbial methanogenesis, which is known to occur in subglacial sediments<sup>37–39</sup>. Some of our lower  $\delta^{13}\text{C}-\text{CH}_4$  suggest this may be occurring in our samples. As found by ref. 40, the introduction of thermogenic methane



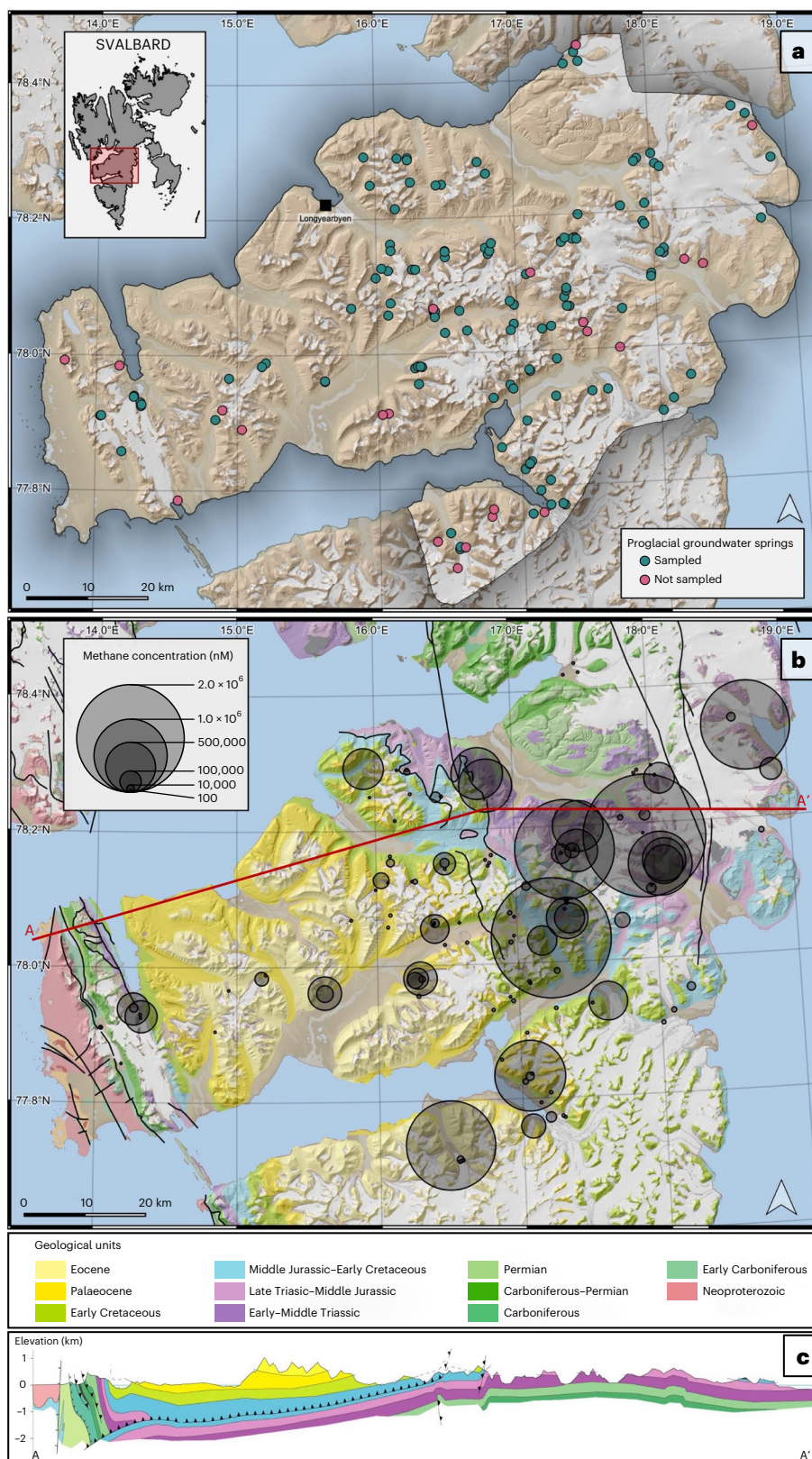


**Fig. 3 | Map of land-terminating glacier sampling locations and corresponding methane concentrations. a**, Map of sampled proglacial groundwater springs (green circles) and springs identified by satellite images but not sampled (pink circles). The outlined area designates the full study region (6,268 km<sup>2</sup>). (The retreat of glacial termini since 1936 can be viewed in ref. 14 to contextualize the magnitude of glacial retreat and the increasing size of the sampled forefields.) **b**, Methane concentrations (nM) of sampled proglacial

groundwater springs displayed by bubble size over a geological map of central Svalbard. Black lines on the map designate the locations of geological faults. The red line indicates the location of the A–A' cross section depicted in **c**. **c**, Cross section displaying the geological layers of the study region. Basemaps in **a**, **b** adapted with permission under a Creative Commons license [CC BY 4.0](https://creativecommons.org/licenses/by/4.0/). Panel **c** adapted with permission ref. 49 under a Creative Commons license [CC BY](https://creativecommons.org/licenses/by/4.0/).

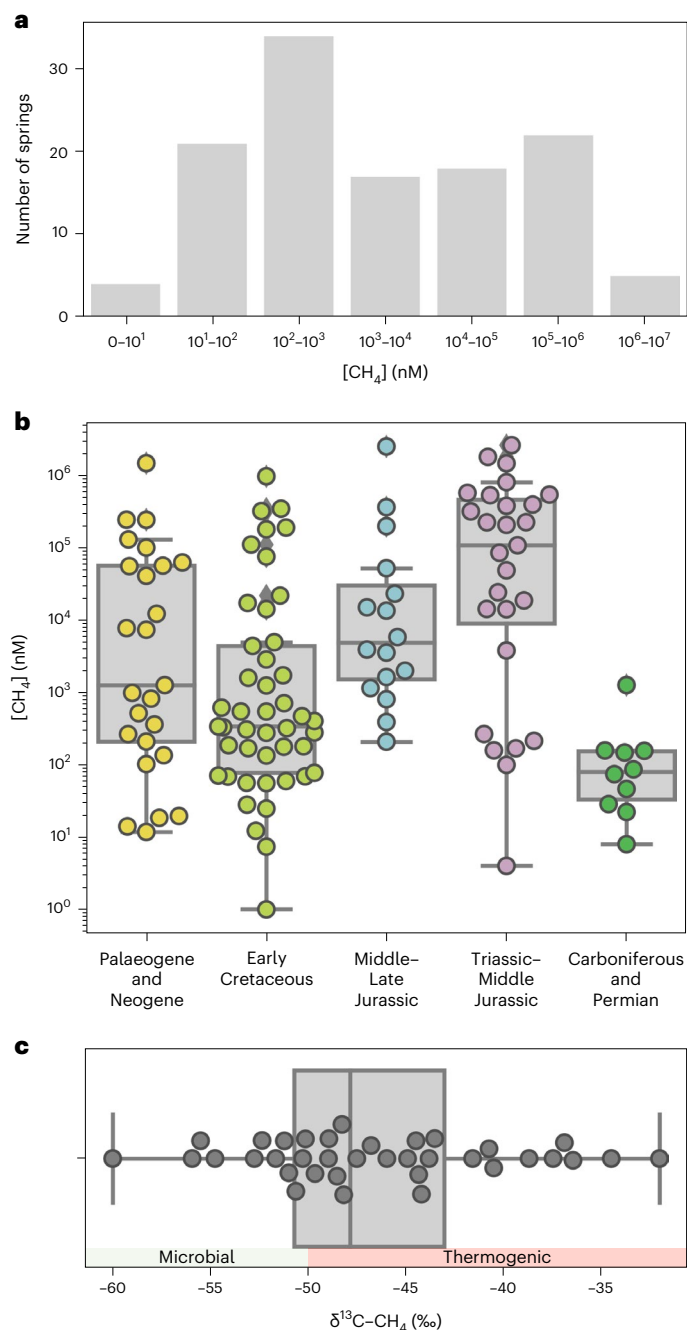


**Fig. 4 | Methane concentrations and carbon isotopic compositions of methane in proglacial groundwaters.** **a**, Histogram of measured methane concentrations in proglacial springs (nM,  $n = 123$ ). Note: log scale on the x axis. **b**, Methane concentrations sorted by outcropping geology at the sampling site. Note: log scale on the y axis. (Palaeogene and Neogene:  $n = 25$ ; Early Cretaceous:  $n = 45$ ; Middle-Late Jurassic:  $n = 16$ ; Triassic-Middle Jurassic:  $n = 27$ ; Carboniferous and Permian:  $n = 10$ .) **c**, Distribution of  $\delta^{13}\text{C}-\text{CH}_4$  values of sampled groundwaters with high enough methane concentrations for isotopic analysis ( $n = 36$ ). In **b, c**, boxes range from the 25th percentile to the 75th percentile; the line across the box represents the median; the whiskers extend to the maximum and minimum values; circles beyond this range represent outliers.

or reduced gases to the subglacial system can reduce the oxidative capacity of the water, thus facilitating the onset of methanogenesis at the glacier bed. This additional source of methane would push the carbon isotopic composition lower, towards the microbial range. It must also be considered that methanotrophy, a microbially mediated methane removal process that can be effective in subglacial sediments<sup>39,41</sup>,

may alternatively shift the isotopic composition of largely microbial methane into the thermogenic realm. However, the abundance of methanotrophs in subglacial environments has been found to be limited by low concentrations of oxygen, iron, nitrate, sulfate or other suitable electron acceptors that are essential to aerobic or anaerobic methane oxidation<sup>37</sup>. Thus, it is not likely that methanotrophy substantially impacts the carbon isotopic composition of our samples, as these groundwaters are limited in electron acceptors coupled to methane oxidation and may not be conducive for methanotrophic communities. It cannot be ruled out, however, and therefore the methane concentrations absent methanotrophy may be higher.

## Methane emissions estimation

Total potential methane emissions from proglacial groundwater springs of land-terminating glaciers within the study region (6,268 km<sup>2</sup>, outlined in Fig. 3a) are estimated with a Monte Carlo simulation, where we apply the aqueous methane concentrations to a corresponding discharge rate. The discharge rate across the freezing season is calculated from the icing area at each sampled site (measured with satellite imagery), the average icing depth (estimated by ground-penetrating radar (GPR)), an assumed ice density (0.917 g cm<sup>-3</sup>) and the number of days below freezing during which the icing was formed. The discharge rates are extrapolated across the year to estimate annual emissions. Icings identified within the region by satellite imagery that were not sampled ( $n = 22$ ; Fig. 3a) are included in the calculation using the measured icing area, the average icing thickness and the average methane concentration of all sampled proglacial springs.

Expected annual emissions from proglacial springs within the region range from 27 t yr<sup>-1</sup> CH<sub>4</sub> ( $\pm 0.14$  t) to 230 t yr<sup>-1</sup> CH<sub>4</sub> ( $\pm 1.1$  t), which equates to emissions of up to 37 kg km<sup>-2</sup> yr<sup>-1</sup> CH<sub>4</sub> ( $\pm 2$  kg km<sup>-2</sup> yr<sup>-1</sup> CH<sub>4</sub>). When we extrapolate this across the Svalbard archipelago without accounting for regional differences in geology, methane emissions associated with proglacial groundwater springs could be up to 2.31 kt yr<sup>-1</sup> CH<sub>4</sub> ( $\pm 0.14$  kt yr<sup>-1</sup> CH<sub>4</sub>). These emissions are comparable to the speculative annual methane flux from glacial run-off for the entire Greenland Ice Sheet, which has been projected as 2.1 kt yr<sup>-1</sup> CH<sub>4</sub> (based on measurements from one outlet glacier)<sup>42</sup>. This is notable, especially as our emissions estimate focuses only on proglacial groundwaters and does not account for summer methane fluxes associated with glacial run-off. A further regional comparison is that our methane emission estimate is equivalent to 8% of Norway's annual oil- and gas-related anthropogenic energy emissions<sup>43</sup>.

These emission estimates assume that all methane exceeding the atmospheric equilibrium concentration is degassed from the groundwater after it is released from the spring and is exposed to the atmosphere. Given that the groundwater flows in a thin film over the icing surface before freezing, the large surface-area-to-volume ratio of the outflow will facilitate rapid outgassing<sup>44</sup>. In addition, the waters are notably clear with no suspended particulate matter to host biologically mediated methane oxidation. Therefore, we expect that the rate of any oxidation within the water is negligible compared with the rate at which methane is outgassed and emitted to the atmosphere<sup>45</sup>, and thus our assumption that all methane outgasses provides a reasonable emission estimate.

## Marine-terminating glaciers as future emission sources

We have focused mainly on land-terminating glaciers, but much of the glaciated regions of the Arctic are dominated by marine-terminating glaciers. Glaciers that terminate in the sea reveal subsea forefields as they retreat. Groundwaters released in these forefields are less likely to be important in terms of atmospheric methane emissions due to oxidative processes within the water column that are effective at removing methane before it reaches the atmosphere, especially aerobic methanotrophy<sup>46</sup>. However, over the past two decades, more than 7% of the



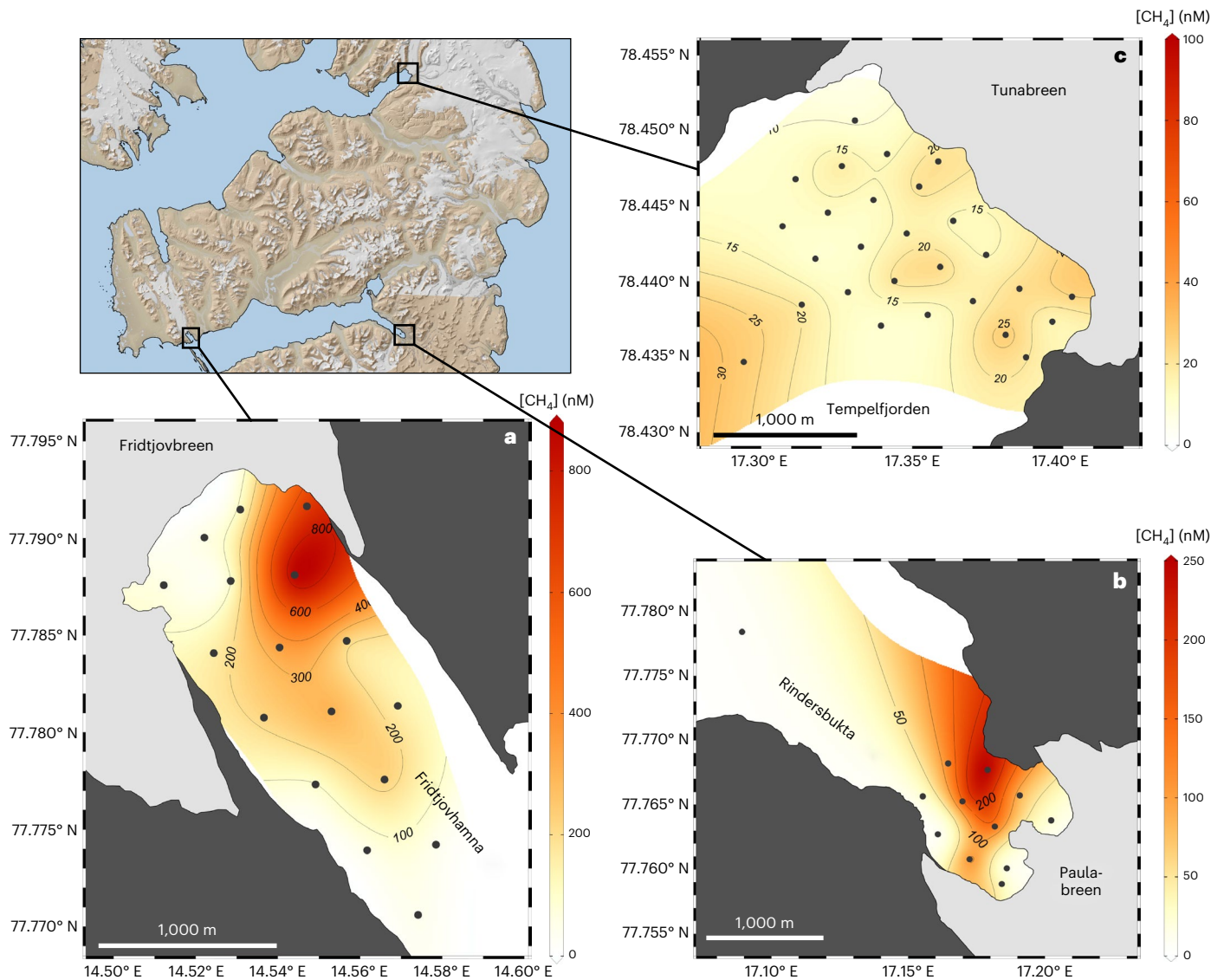


**Fig. 5 | Surface-water methane concentrations of fjords adjacent to marine-terminating glaciers.** Methane concentrations (nM) are denoted by coloured shading on the maps and are interpolated from the sampling points (grey dots) using Data-Interpolating Variational Analysis. Note the different concentration scale on each map. Concentrations are displayed for subsea-ice surface waters adjacent to three marine-terminating glaciers (glaciers are light grey; land is

dark grey). **a**, Fridtjovbreen (Triassic–Middle Jurassic). **b**, Paulabreen (Early Cretaceous). **c**, Tunabreen (Carboniferous and Permian). Water depths are less than 60 m. Land and glacier shapefiles were digitalized manually by tracing Sentinel-2 satellite images. Figure created with Ocean Data View (<https://odv.awi.de>).

Arctic's 1,704 marine-terminating glaciers have lost enough mass that their termini have retreated and are now completely on land<sup>47</sup>. As this trend continues, more marine-terminating glaciers will present novel methane emission sites by revealing new onshore glacial forefields during the retreat of their termini onto land.

We investigate whether methane-rich groundwater springs will be active in these newly formed forefields by measuring methane concentrations in fjord surface waters adjacent to three marine-terminating glaciers in central Svalbard. Our analysis reveals areas of supersaturated methane (concentrations up to 876 nM, compared with marine equilibrium concentrations of ~3.3 nM) in front of all three glaciers (Fig. 5). The high methane concentrations are not correlated with low salinity (Supplementary Fig. 1) as would be expected if the methane was sourced from the dilute, high-volume subglacial meltwater plume as opposed to seepage from deeper sources via the seafloor. This leads us to conclude that the methane is sourced from groundwater seeps within the subsea forefields of the glaciers. We find that the marine-terminating glaciers

follow a similar geological dependency of methane concentrations as the proglacial springs of land-terminating glaciers. The glacier located in a region with shale-dominated Jurassic and Triassic formations (Fridtjovbreen; Fig. 5a) exhibits much higher methane concentrations in its adjacent fjord waters than the glacier lying in Early Cretaceous formations (Paulabreen; Fig. 5b) and even more than that in Carboniferous and Permian formations (Tunabreen; Fig. 5c).

We propose that methane emissions from marine-terminating glaciers will increase as the glaciers retreat, first as the termini move to shallower waters and the newly exposed forefields are submerged under a shallow water column where methane is less exposed to oxidative processes. Subsequently, emissions will continue to increase with further retreat of the termini onto land as terrestrial seepage points begin to form with direct emissions to the atmosphere. Marine-terminating glaciers may become substantial new methane emission sources across the Arctic as they continue to lose mass due to increasing Arctic air temperatures.

The observed pace of warming in the Arctic has far exceeded climate model predictions, probably due to many feedback loops within the Arctic that the models fail to capture<sup>48</sup>. Our findings present a regionally important feedback loop related to climate-driven glacier melt that is currently not considered in the Arctic methane budget, where rapid glacial retreat is opening new pathways for methane escape. As Svalbard is warming at a rate more than twice the Arctic average<sup>13</sup>, its responses to warming are indicators of what can be expected in other regions of the Arctic and Antarctica. Improving our understanding of possible pan-Arctic methane release from proglacial groundwater springs is necessary to assess the importance of such emissions and their potential global climate impact. This is particularly relevant in regions where glaciers are capping large reservoirs of geologic methane, such as parts of Arctic Canada and the Russian Arctic<sup>1</sup>, where further melting of the cryosphere could lead to considerable seeps of this potent greenhouse gas.

## Online content

Any methods, additional references, Nature Portfolio reporting summaries, source data, extended data, supplementary information, acknowledgements, peer review information; details of author contributions and competing interests; and statements of data and code availability are available at <https://doi.org/10.1038/s41561-023-01210-6>.

## References

- Gautier, D. L. et al. Assessment of undiscovered oil and gas in the Arctic. *Science* **324**, 1175–1179 (2009).
- Isaksen, I. S. A., Gauss, M., Myhre, G., Walter Anthony, K. M. & Ruppel, C. Strong atmospheric chemistry feedback to climate warming from Arctic methane emissions. *Glob. Biogeochem. Cycles* **25**, GB2002 (2011).
- Lerche, I., Yu, Z., Tørudbakken, B. & Thomsen, R. O. Ice loading effects in sedimentary basins with reference to the Barents Sea. *Mar. Pet. Geol.* **14**, 277–338 (1997).
- Walter Anthony, K. M., Anthony, P., Grosse, G. & Chanton, J. Geologic methane seeps along boundaries of Arctic permafrost thaw and melting glaciers. *Nat. Geosci.* **5**, 419–426 (2012).
- Lacroix, A. V. Unaccounted-for sources of fossil and isotopically-enriched methane and their contribution to the emissions inventory: a review and synthesis. *Chemosphere* **26**, 507–557 (1993).
- Collett, T. S. et al. Permafrost-associated natural gas hydrate occurrences on the Alaska North Slope. *Mar. Pet. Geol.* **28**, 279–294 (2011).
- Kohnert, K., Serafimovich, A., Metzger, S., Hartmann, J. & Sachs, T. Strong geologic methane emissions from discontinuous terrestrial permafrost in the Mackenzie delta, Canada. *Sci. Rep.* **7**, 5828 (2017).
- Shakhova, N. et al. Extensive methane venting to the atmosphere from sediments of the East Siberian Arctic Shelf. *Science* **327**, 1246–1250 (2010).
- Wallmann, K. et al. Gas hydrate dissociation off Svalbard induced by isostatic rebound rather than global warming. *Nat. Commun.* **9**, 83 (2018).
- Berndt, C. et al. Temporal constraints on hydrate-controlled methane seepage off Svalbard. *Science* **343**, 284–287 (2014).
- Portnov, A., Vadakkepulyambatta, S., Mienert, J. & Hubbard, A. Ice-sheet-driven methane storage and release in the Arctic. *Nat. Commun.* **7**, 10314 (2016).
- Sullivan, T. D. et al. Influence of permafrost thaw on an extreme geologic methane seep. *Permafr. Periglac. Process.* **32**, 484–502 (2021).
- Isaksen, K. et al. Exceptional warming over the Barents area. *Sci. Rep.* **12**, 9371 (2022).
- Geyman, E. C., van Pelt, W. J. J., Maloof, A. C., Aas, H. F. & Kohler, J. Historical glacier change on Svalbard predicts doubling of mass loss by 2100. *Nature* **601**, 374–379 (2022).
- Svendsen, J. I. & Mangerud, J. Holocene glacial and climatic variations on Spitsbergen, Svalbard. *Holocene* **7**, 45–57 (1997).
- Moorman, B. J. Glacier–permafrost hydrological interconnectivity: Stagnation Glacier, Bylot Island, Canada. *Geol. Soc. Lond. Spec. Publ.* **242**, 63–74 (2005).
- Wainstein, P., Moorman, B. & Whitehead, K. Glacial conditions that contribute to the regeneration of Fountain Glacier proglacial icing, Bylot Island, Canada. *Hydrol. Process.* **28**, 2749–2760 (2014).
- Bukowska-Janina, E. & Szafranec, J. Distribution and morphometric characteristics of icing fields in Svalbard. *Polar Res.* **24**, 41–53 (2005).
- Mallinson, L., Swift, D. A. & Sole, A. Proglacial icings as indicators of glacier thermal regime: ice thickness changes and icing occurrence in Svalbard. *Geogr. Ann. Ser. A* **101**, 334–349 (2019).
- Yde, J. C. & Knudsen, N. T. Observations of debris-rich naled associated with a major glacier surge event, Disko Island, West Greenland. *Permafr. Periglac. Process.* **16**, 319–325 (2005).
- Chesnokova, A., Baraër, M. & Bouchard, É. Proglacial icings as records of winter hydrological processes. *Cryosphere* **14**, 4145–4164 (2020).
- Betlem, P., Senger, K. & Hodson, A. 3D thermobaric modelling of the gas hydrate stability zone onshore central Spitsbergen, Arctic Norway. *Mar. Pet. Geol.* **100**, 246–262 (2019).
- Hodson, A. J. et al. Sub-permafrost methane seepage from open-system pingos in Svalbard. *Cryosphere* **14**, 3829–3842 (2020).
- McGuire, A. D. et al. Sensitivity of the carbon cycle in the Arctic to climate change. *Ecol. Monogr.* **79**, 523–555 (2009).
- Ohm, S. E. et al. Discovery of shale gas in organic rich Jurassic successions, Adventdalen, Central Spitsbergen, Norway. *Nor. Geol. Tidsskr.* **99**, 349–376 (2019).
- Liira, M. et al. Sediment geochemical study of hydrocarbon seeps in Isfjorden and Mohnbukta: a comparison between western and eastern Spitsbergen, Svalbard. *arktos* **5**, 49–62 (2019).
- Knies, J., Damm, E., Gutt, J., Mann, U. & Pinturier, L. Near-surface hydrocarbon anomalies in shelf sediments off Spitsbergen: evidences for past seepages. *Geochem. Geophys. Geosyst.* **5**, Q06003 (2004).
- Roy, S., Hovland, M., Noormets, R. & Olausson, S. Seepage in Isfjorden and its tributary fjords, West Spitsbergen. *Mar. Geol.* **363**, 146–159 (2015).
- Damm, E., Mackensen, A., Budéus, G., Faber, E. & Hanfland, C. Pathways of methane in seawater: plume spreading in an Arctic shelf environment (SW-Spitsbergen). *Cont. Shelf Res.* **25**, 1453–1472 (2005).
- Abay, T. B. et al. Migrated petroleum in outcropping Mesozoic sedimentary rocks in Spitsbergen: organic geochemical characterization and implications for regional exploration. *J. Pet. Geol.* **40**, 5–36 (2017).
- Hammer, Ø. et al. Hydrocarbon seeps from close to the Jurassic–Cretaceous boundary, Svalbard. *Palaeogeogr. Palaeoclimatol. Palaeoecol.* **306**, 15–26 (2011).
- Nøttvedt, A., Livbjerg, F., Midbøe, P. S. & Rasmussen, E. Hydrocarbon potential of the Central Spitsbergen Basin. *Norwegian Petroleum Society Special Publications* **2**, 333–361 (Elsevier, 1993).
- Abay, T. B. Source rocks at Svalbard: an overview of Jurassic and Triassic formations and comparison with offshore Barents Sea time equivalent source rock formations. *AAPG Datapages Search and Discovery.* **30372**, 1–23 (2014).

34. Rodes, N. et al. From source rocks to the surface: the fate of gas seepage in high Arctic fjords, Svalbard. In *Proc. 83rd EAGE Annual Conference & Exhibition*. **2022**, 1–5 (European Association of Geoscientists & Engineers, 2022).
  35. Roy, S. et al. Fluid migration pathways to seafloor seepage in inner Isfjorden and Adventfjorden, Svalbard. *Nor. Geol.* **94**, 99–119 (2014).
  36. Whiticar, M. J. Carbon and hydrogen isotope systematics of bacterial formation and oxidation of methane. *Chem. Geol.* **161**, 291–314 (1999).
  37. Stibal, M. et al. Methanogenic potential of Arctic and Antarctic subglacial environments with contrasting organic carbon sources. *Glob. Change Biol.* **18**, 3332–3345 (2012).
  38. Wadham, J. L., Tranter, M., Tulaczyk, S. & Sharp, M. Subglacial methanogenesis: a potential climatic amplifier? *Glob. Biogeochem. Cycles* **22**, GB2021 (2008).
  39. Dieser, M. et al. Molecular and biogeochemical evidence for methane cycling beneath the western margin of the Greenland Ice Sheet. *ISME J.* **8**, 2305–2316 (2014).
  40. Burns, R. et al. Direct isotopic evidence of biogenic methane production and efflux from beneath a temperate glacier. *Sci. Rep.* **8**, 17118 (2018).
  41. Michaud, A. B. et al. Microbial oxidation as a methane sink beneath the West Antarctic Ice Sheet. *Nat. Geosci.* **10**, 582–586 (2017).
  42. Lamarche-Gagnon, G. et al. Greenland melt drives continuous export of methane from the ice-sheet bed. *Nature* **565**, 73–77 (2019).
  43. Methane Tracker, IEA, <https://www.iea.org/data-and-statistics/data-tools/methane-tracker> (2023).
  44. Heilweil, V. M., Solomon, D. K., Darrah, T. H., Gilmore, T. E. & Genereux, D. P. Gas-tracer experiment for evaluating the fate of methane in a coastal plain stream: degassing versus in-stream oxidation. *Environ. Sci. Technol.* **50**, 10504–10511 (2016).
  45. Rovelli, L. et al. Contrasting biophysical controls on carbon dioxide and methane outgassing from streams. *J. Geophys. Res. Biogeosci.* **127**, e2021JG006328 (2022).
  46. Mau, S. et al. Widespread methane seepage along the continental margin off Svalbard—from Bjørnøya to Kongsfjorden. *Sci. Rep.* **7**, 42997 (2017).
  47. Kochtitzky, W. & Copland, L. Retreat of Northern Hemisphere marine-terminating glaciers, 2000–2020. *Geophys. Res. Lett.* **49**, e2021GL096501 (2022).
  48. Rantanen, M. et al. The Arctic has warmed nearly four times faster than the globe since 1979. *Commun. Earth Environ.* **3**, 168 (2022).
  49. Dallmann, W. K. *Geological Map of Svalbard (1:750000)* (Norwegian Polar Institute, 2014).
- Publisher's note** Springer Nature remains neutral with regard to jurisdictional claims in published maps and institutional affiliations.
- Open Access** This article is licensed under a Creative Commons Attribution 4.0 International License, which permits use, sharing, adaptation, distribution and reproduction in any medium or format, as long as you give appropriate credit to the original author(s) and the source, provide a link to the Creative Commons license, and indicate if changes were made. The images or other third party material in this article are included in the article's Creative Commons license, unless indicated otherwise in a credit line to the material. If material is not included in the article's Creative Commons license and your intended use is not permitted by statutory regulation or exceeds the permitted use, you will need to obtain permission directly from the copyright holder. To view a copy of this license, visit <http://creativecommons.org/licenses/by/4.0/>.
- © The Author(s) 2023



## Methods

### Proglacial groundwater spring sampling and analysis

Field samples for groundwater methane concentrations were collected between February and May of both 2021 and 2022. Sampling locations are detailed in Fig. 3a and the Supplementary Data and represent winter icings of 78 glaciers across central Svalbard. Proglacial groundwater springs were reached by drilling into ice blisters (large, upheaved dome features of ice formed by pressurized water flow beneath or within the icing; Fig. 2b) on winter icings with a 7-cm-diameter auger until pressurized water was released. Unfiltered samples for methane analysis were taken directly from the spring outlet in 22 ml gas-tight serum vials, ensuring they were bubble-free before sealing shut. Samples were spiked within 24 h with 1 ml of 1 M NaOH while concurrently removing 1 ml of sample to stop microbial activity. Samples were stored upside down in the dark at 4 °C until analysis.

A headspace of 4 ml pure N<sub>2</sub> gas was created in each vial, and samples were left to equilibrate at room temperature for at least 24 h. The concentration of methane in the headspace was measured at Queen Mary University of London by gas chromatography fitted with a flame ionization detector (Agilent Technologies UK Ltd). Calibration gas standards (100 ppm CH<sub>4</sub>; BOC Limited) and ambient air were analysed in each analytical sequence and repeated at regular intervals to check for drift. The total amount of methane in each sample (headspace and water phase) was calculated using the ideal gas law and solubility coefficients from ref. 50 (Supplementary Information). Stable carbon isotope ratios of methane (δ<sup>13</sup>C–CH<sub>4</sub>) in samples with sufficiently high methane concentrations were analysed at the University of Cambridge in the LASER-ENVI facility using a cavity ringdown spectrometer (Picarro G2201-I, Picarro Inc.) and reported relative to the Vienna Pee Dee Belemnite standard.

### Icing depth measurements

Radio echo sounding with GPR equipment was used to obtain icing thickness measurements, which were further validated by manual auger drillings. The GPR surveys were performed using a Malå ProEx control unit, 800 MHz, 500 MHz and 100 MHz antennas (changed due to equipment availability over the field season) and a generic USB (universal serial bus) GNSS (global navigation satellite system) receiver. A total of 29 km of lines was surveyed over 11 discrete proglacial icings during spring 2022, and 25 validation points along the GPR track were drilled manually. Post-processing of the GPR data included time-zero correction, horizontal and vertical resolution standardization, topographic Kirchhoff migration<sup>51</sup> with a medium velocity of clean ice (0.168 m ns<sup>-1</sup>) and automatic gain control. The correlation between the digitized radargrams and the manual auger drillings was significant ( $R^2 = 0.74$ ), with no apparent bias, which validates that the correct reflection was digitized and the medium velocity of clean ice is accurate.

### Methane emission calculations

**Icing volume calculations.** Icing thickness measurements obtained by GPR surveys were used to determine an average ice depth across all icings. Areas of each glacial icing were measured on Sentinel-2 satellite images from May 2021 and April 2022 using the polygon feature in the geographic information system application QGIS. Measurements were repeated three times on separate days to determine an error for the measurement. Icing areas were multiplied by the average icing depth to obtain an icing volume at each glacial site.

**Monte Carlo simulation.** A Monte Carlo simulation, run 10,000 times for each icing, was used to calculate a range of potential emissions from each glacial site. The Monte Carlo sampling was taken from a normal distribution according to the defined errors of each parameter (Supplementary Data). Maximum and minimum emission scenarios were considered for each glacier, in which the maximum measured methane concentration and icing area were used for the highest emission

scenario and the minimum concentration and icing area were used in the lowest emission scenario. These emissions were summed to determine maximum and minimum total methane fluxes from the full study region.

Annual methane emissions for each glacial icing were estimated using the following equation:

$$f_{\text{CH}_4,i} = \frac{A_{\text{icing},i} \times d_{\text{icing(avg)}} \times \rho_{\text{ice}} \times ([\text{CH}_4]_i - [\text{CH}_4]_{\text{(eq)}})}{n_{\text{days of icing formation},i}} \times 365.24$$

where  $f_{\text{CH}_4,i}$  is the annual flux of methane from the glacial icing  $i$ ,  $A_{\text{icing},i}$  is the measured area of the icing  $i$ ,  $d_{\text{icing(avg)}}$  is the average thickness of all icings determined by GPR,  $\rho_{\text{ice}}$  is the density of ice (0.917 g cm<sup>-3</sup>),  $[\text{CH}_4]_i$  is the aqueous methane concentration of the formation water of the icing  $i$ ,  $[\text{CH}_4]_{\text{(eq)}}$  is the equilibrium concentration of methane in water at 0 °C and 1 atm (4 nM) and  $n_{\text{days of icing formation},i}$  is the number of days between the onset of constant freezing air temperatures in the previous year to the date of the satellite image used to calculate the icing area.

**Assumptions made for the Monte Carlo simulation.** In the calculations, we assumed that the total discharge from the proglacial groundwater spring since the onset of freezing temperatures has been trapped frozen in the icing, and thus the icing volume can be used as a proxy of total discharge over this period. We also made the conservative assumption in our calculations that this discharge rate is constant year-round. Finally, it is assumed that the aqueous methane concentrations of the proglacial springs are constant throughout the year. Limited data collected in summer from a subset of the sites support this simplification (Supplementary Data). All assumptions made are listed in the following, and all errors considered in the calculations are provided in the Supplementary Data.

- Groundwater spring discharge rate is constant throughout the year.
- All methane above the ~4 nM equilibrium concentration will be emitted to the atmosphere.
- Measured concentrations represent the methane concentrations throughout the year for each spring sampled.
- Measured methane concentrations represent the concentrations of all groundwater that has formed the icing.
- All icings have a similar average depth, within the range of error.
- All discharge from the groundwater spring since the onset of freezing until the date of area measurement has been trapped within the icing.
- Any snow incorporated within the icing is negligible.
- Any saturated sediments below the icing are negligible in terms of discharge water volume.
- Samples taken from the same location but on different days are from the same groundwater source, and their methane concentrations can be averaged.
- Samples taken from different locations within the icing represent different groundwater springs if their water chemistries are different.
- Water samples have not been freeze-concentrated or diluted by inclusion of snow around the icing.
- The addition of NaOH to each sample has ceased any microbial activity that may otherwise have altered the methane concentrations during sample storage.
- Satellite imagery captures the full icing.
- Density of all icing ice is 0.917 g cm<sup>-3</sup>.
- All glacial icings within the selected region have been identified and are represented in the calculations.
- The entirety of the previous year's icing melted before the new icing began to form (satellite imagery confirms that this is largely the case).

**Handling of icings that were not sampled.** Twenty-two glacial icings that were not sampled were identified in the sampling region by satellite imagery (Fig. 3a). These icings were included in the Monte Carlo simulation to consider emissions from all proglacial groundwater springs in the study region. Icing volumes of these sites were determined following the preceding approach. An average methane concentration from all sampled proglacial groundwater springs was used in place of a measured methane concentration for each of the unsampled sites to calculate a methane flux and estimate their potential contribution to a regional methane flux.

**Limitations in the method.** Our method for calculating methane emissions is likely to underestimate the discharge rates of the groundwater springs due to challenges in assessing the icing volume. As satellite imagery is used to measure the icing area, it is not possible to determine whether sections are snow covered, and therefore large areas of the icings may be left out of the measurements. In addition, the GPR surveys used to determine an average icing thickness were conducted between late March and early May, before growth of the icing was complete. This means that the measurements do not represent the maximum depth reached by the icing during the winter season and therefore underestimate total discharge.

### Sampling and analysis of fjord surface waters

Sampling of fjord surface waters adjacent to marine-terminating glaciers was completed in April and May of 2021 while the fjords were still covered by sea ice. Samples were taken in a high-spatial-resolution grid pattern in front of the glaciers and were acquired by drilling holes through the sea ice and using a bailer to retrieve surface water from beneath the ice. Samples for methane concentration analysis were transferred into 100 ml gas-tight serum vials using a syringe, ensuring they were bubble-free before sealing. Electrical conductivity measurements were taken in the field with a Hach probe. Upon return from the field, samples for methane concentration measurements were spiked with 1 ml of 1 M NaOH and stored upside down in the dark at 4 °C until analysis. Before analysis, a headspace of 5 ml N<sub>2</sub> was created, replacing 5 ml of sample, and left to equilibrate for more than 24 h at room temperature. Measurements of methane in the headspace were made at the University of Tromsø with a ThermoScientific GC Trace gas chromatograph fitted with a flame ionization detector and an MSieve 5 A column (ThermoScientific). Calculations of methane concentrations were handled as described in the Supplementary Information, while also accounting for salinity.

### Statistical analysis

Statistical analysis was performed in RStudio (version 3.4.2). A one-way analysis of variance was used to determine whether bedrock geology was significantly related to methane concentrations of proglacial groundwater springs. Homogeneity and normality were confirmed by visual inspection, and residual plots were used to validate fulfilment of relevant test assumptions. Methane concentrations were log<sub>10</sub>-transformed to meet these requirements. All possible pairwise comparisons were made with Tukey's honestly significant difference post hoc test (Supplementary Table 1).

### Data availability

The methane concentration data that support the findings of this study are available in the Zenodo repository (<https://doi.org/10.5281/zenodo.7709380>).

### References

50. Wiesenburg, D. A. & Guinasso, N. L. Equilibrium solubilities of methane, carbon monoxide, and hydrogen in water and sea water. *J. Chem. Eng. Data* **24**, 356–360 (1979).
51. Dujardin, J.-R. & Bano, M. Topographic migration of GPR data: examples from Chad and Mongolia. *C. R. Geosci.* **345**, 73–80 (2013).

### Acknowledgements

This work was supported by the CLIMAGAS and HYDRO-SURGE projects, both funded by the Research Council of Norway (project no. 294764 (A.J.H.) and 329174 (G.E.K.), respectively). Funding for fieldwork was also provided by the Robert Scott Fund granted by The Geological Society of London (G.E.K.). We thank the governor of Svalbard for granting us access to restricted zones to conduct fieldwork, as well as S. M. Cohen and the rest of the UNIS Logistics team for their field support. We are grateful to M. Gevers, E. Jones, K. Redeker, M. T. Hornum and P. Betlem for their help in the field and valuable discussions on methane fluxes, glacial hydrology and gas hydrate stability zones.

### Author contributions

A.J.H. and G.E.K. designed the study and managed the CLIMAGAS and HYDRO-SURGE grants, respectively. G.E.K., A.J.H., L.M. and E.S.M. conducted the fieldwork. L.M. led the marine-terminating glacier part of the study and conducted the statistical analysis. G.E.K. performed the laboratory analyses. E.S.M. performed the processing of GPR surveys. G.E.K., L.M. and A.J.H. created the figures. G.E.K. and H.J.B. performed the Monte Carlo simulation. A.V.T., M.T. and Y.Z. provided access to and/or support with laboratory instruments. G.E.K. wrote the paper with valuable contributions from all authors.

### Competing interests

The authors declare no competing interests.

### Additional information

**Supplementary information** The online version contains supplementary material available at <https://doi.org/10.1038/s41561-023-01210-6>.

**Correspondence and requests for materials** should be addressed to Gabrielle E. Kleber.

**Peer review information** *Nature Geoscience* thanks Alexey Portnov and Ronald Daanen for their contribution to the peer review of this work. Primary Handling Editor: Xujia Jiang, in collaboration with the *Nature Geoscience* team.

**Reprints and permissions information** is available at [www.nature.com/reprints](http://www.nature.com/reprints).